








Tailoring of surface plasmon resonances in TiN/(Al_{0.72}Sc_{0.28})N multilayers by dielectric layer thickness variation

Magnus Garbrecht^{1,*} , Lars Hultman¹ , Mohammed H. Fawey^{2,3} , Timothy D. Sands^{4,5} , and Bivas Saha⁶ 

¹Thin Film Physics Division, Department of Physics, Chemistry and Biology, Linköping University, 581 83 Linköping, Sweden

²Karlsruhe Institute of Technology (KIT), Institute of Nanotechnology (INT), Hermann-von-Helmholtz-Platz 1, 76344 Eggenstein-Leopoldshafen, Germany

³Joint Research Laboratory Nanomaterials (KIT and TUD) at Technische Universität Darmstadt (TUD), Jovanka-Bontschits-Str. 2, 64287 Darmstadt, Germany

⁴Bradley Department of Electrical and Computer Engineering, Virginia Tech, Blacksburg, VA 24061, USA

⁵Department of Materials Science and Engineering, Virginia Tech, Blacksburg, VA 24061, USA

⁶Department of Materials Science and Engineering, University of California, Berkeley, CA 94720, USA

Received: 20 September 2017

Accepted: 17 November 2017

Published online:

28 November 2017

© The Author(s) 2017. This article is an open access publication

ABSTRACT

Alternative designs of plasmonic metamaterials for applications in solar energy-harvesting devices are necessary due to pure noble metal-based nanostructures' incompatibility with CMOS technology, limited thermal and chemical stability, and high losses in the visible spectrum. In the present study, we demonstrate the design of a material based on a multilayer architecture with systematically varying dielectric interlayer thicknesses that result in a continuous shift of surface plasmon energy. Plasmon resonance characteristics of metal/semiconductor TiN/(Al,Sc)N multilayer thin films with constant TiN and increasing (Al,Sc)N interlayer thicknesses were analyzed using aberration-corrected and monochromated scanning transmission electron microscopy-based electron energy loss spectroscopy (EELS). EEL spectrum images and line scans were systematically taken across layer interfaces and compared to spectra from the centers of the respective adjacent TiN layer. While a constant value for the TiN bulk plasmon resonance of about 2.50 eV was found, the surface plasmon resonance energy was detected to continuously decrease with increasing (Al,Sc)N interlayer thickness until 2.16 eV is reached. This effect can be understood to be the result of resonant coupling between the TiN bulk and surface plasmons across the dielectric interlayers at very low (Al,Sc)N thicknesses. That energy interval between bulk and decreasing surface plasmon resonances corresponds to wavelengths in the visible spectrum. This shows the potential of tailoring the material's plasmonic response by controlling the (Al,Sc)N interlayer thickness,

Address correspondence to E-mail: magnus.garbrecht@liu.se

making TiN-based multilayers good prospects for plasmonic metamaterials in energy devices.

Introduction

Plasmonic resonances are collective, coherent excitations of a metal's conduction electrons stimulated by incident electromagnetic waves [1]. Surface plasmons of metallic nanostructures localize light below the diffraction limit and can generate intense electric near fields with well-defined resonances within the optical window [2, 3]. Applications exploiting this unique effect include single-molecule spectroscopy, molecular sensors, photothermal cancer therapy, photocatalytics, and photovoltaics, the latter due to the enhancement of efficiency in hot-electron-based solar energy-harvesting devices [4–9]. Plasmonic nanostructures comprise hitherto mostly noble metals like gold and silver, which unfortunately are not compatible with standard CMOS (complementary metal-oxide semiconductor) technology due to their limited chemical and thermal stability and difficulty in depositing them as smooth continuous thin films. Moreover, noble metals limit the efficiency in applications due to characteristic losses from interband transitions in the optical range [10, 11].

Alternative approaches such as the use of Al and noble metal alloys have been demonstrated [12, 13]. Suffering from similar losses but being fully compatible with commonly used growth technology, as an alternative to noble metals, the extraordinarily temperature stable and chemically inert refractory transition metal nitrides like TiN have been found to exhibit plasmonic properties similar to gold [14–17]. Designs for plasmon induced hot-electron photovoltaics have been most recently demonstrated [18–20], including theoretical reports that shown that metal/semiconductor layered structured could indeed demonstrate higher performances in such photovoltaic devices in comparison with a bilayer metal/semiconductor structure [21].

Moreover, it was demonstrated that transition metal nitrides such as TiN can be grown as a constituent of single-crystal thin-film epitaxial metal/semiconductor superlattices with low defect densities exhibiting high melting points and mechanical hardness for applications as hard coatings and high-temperature

thermoelectric materials [22–28]. In addition to its high chemical and thermal stability, a TiN/(Al,Sc)N multilayer architecture with metal/dielectric interfaces has been proven a promising hyperbolic metamaterial in the visible spectral range and demonstrated large enhancement of its densities of photon states which could be useful in various quantum electronic and optoelectronic applications [29, 30].

While it is known that single TiN thin films show two discrete plasmon resonances for their bulk and surface components [17], tailoring the plasmonic response of TiN is essential for designing high-efficiency hot-electron photovoltaic, photocatalytic, and other devices. The aim of this study is to (a) demonstrate the design of a material based on a superlattice architecture with systematically varying dielectric interlayer thicknesses that result in a continuous shift of the TiN surface plasmon energy and (b) to understand the effects of the dielectric spacer layer thickness on the plasmonic properties of TiN. Changes in the plasmonic resonance energies of TiN with respect to $\text{Al}_{0.72}\text{Sc}_{0.28}\text{N}$ dielectric spacer layer thickness in a lattice-matched epitaxial low-defect metal/dielectric heterostructure will broaden the spectral range of its operation and is expected to enhance the efficiency of the devices. It must also be remembered that such analysis and engineering of the plasmon resonance would unlikely be achieved with noble metals since it is hard to develop a noble metal-based epitaxial metal/dielectric heterostructure with low defect densities.

The plasmonic responses were mapped by state-of-the-art scanning transmission electron microscopy (STEM)-based electron energy loss spectroscopy (EELS). EELS is widely used as a standard technique for characterization of plasmonic materials, due to its combined high-spectral and sub-Ångström spatial resolution, which is required for nanometer-sized material structures.

Experimental

Film growth and treatment

Epitaxial, nominally monocrystalline TiN/(Al,Sc)N metal/dielectric multilayers with rock salt crystal

structure were deposited on (001)-oriented MgO substrates at 750 °C in a 10 mTorr Ar/N₂ (4 sccm Ar/ 6 sccm N₂) ambient via reactive dc-magnetron sputtering (PVD Products, Inc.) from scandium (99.998% purity), aluminum (99.99%), and titanium (99.99%) targets in a top-down confocal arrangement. The growth chamber was equipped with four targets and three DC power supplies, and the base pressure was $< 7 \times 10^{-6}$ Pa (5×10^{-8} Torr) prior to deposition. The magnetron sputtering was performed in constant power mode (with Al = 200 W; Sc = 180 W; Ti = 200 W) with a target to substrate distance of 9 cm and a substrate rotation speed of 5 rpm. While the thickness of all TiN layers was aimed to a constant 20 nm, the lowermost (Al,Sc)N layer thickness was 2 nm and from there increased in steps of 2 nm with each additional layer until the (Al,Sc)N thickness reached 20 nm, so that the resulting stack features a sequence of: MgO substrate/20 nm TiN/2 nm (Al,Sc)N/20 nm TiN/4 nm (Al,Sc)N/20 nm TiN/6 nm (Al,Sc)N/20 nm TiN/8 nm (Al,Sc)N, and so forth, as is shown in the cross-sectional STEM micrograph in Fig. 1.

In order to assure epitaxial growth of the multilayers, lattice match was achieved by yielding a dielectric layer stoichiometry of Al_{0.72}Sc_{0.28}N and TiN_{*x*} with *x* = 1, which was confirmed by energy-dispersive X-ray spectroscopy (EDS) measurements in the TEM with an error of about 2%. The epitaxial growth is confirmed by the selected area electron

diffraction pattern (SAED) shown in the inset of Fig. 1.

Electron microscopy methods and EEL spectra acquisition and analysis

All STEM and EELS experiments were conducted with the Linköping image- and probe-corrected and monochromated FEI Titan³ 60-300 microscope equipped with a Gatan ERS Quantum GIF, high-brightness XFEG source, and dual-EELS fast-shutter system, operated at 300 kV. Using the probe corrector, the spatial resolution achieved was better than 1 Å. By exciting the monochromator and setting the finest available spectrometer dispersion of 0.01 eV/channel, the energy resolution was kept at about 0.2 eV as measured by full-width at half-maximum of the zero-loss peak (ZLP) at 1 s exposure.

The probe current during EELS spectrum acquisition was about 150 pA, and analysis of the low-loss region was done by background removal via fitting a power law decay function to the ZLP tails. After background subtraction, Gauss plots were fitted to the individual peaks for determination of TiN surface plasmon energy E_p . All data analysis was done using Gatan Digital Micrograph.

In order to account for sample drift, the fast-scan direction is chosen to be parallel to the interfaces, and several pixels were binned together in the same direction. The spectra are normalized to take current changes into account. No other algorithms have been applied to further smoothen the line spectra.

EDS maps were recorded with a Super-X EDS detector system for ultra-high count rates in STEM mode, and EDS maps with total counts well above 1.000.000 have been recorded for quantification to confirm both the TiN and Al_{0.72}Sc_{0.28}N layer composition. Each of these spectra can be quantified individually or by combining any number of spectra in, e.g., a line or box, as shown in the supplementary information Figure S1. Hence, for quantification about $250 \times 250 = 62500$ full spectra for each map could be used to become integrated in any possible way and analyzed. Binning thousands of those (ZAF-corrected) spectra together and applying the *k*-factor method yield a precision better than 2% to confirm TiN_{*x*} with *x* = 1. That precision is even higher for the Al_{0.72}Sc_{0.28}N composition since Al and Sc differ less in atomic number and have no peak overlaps.

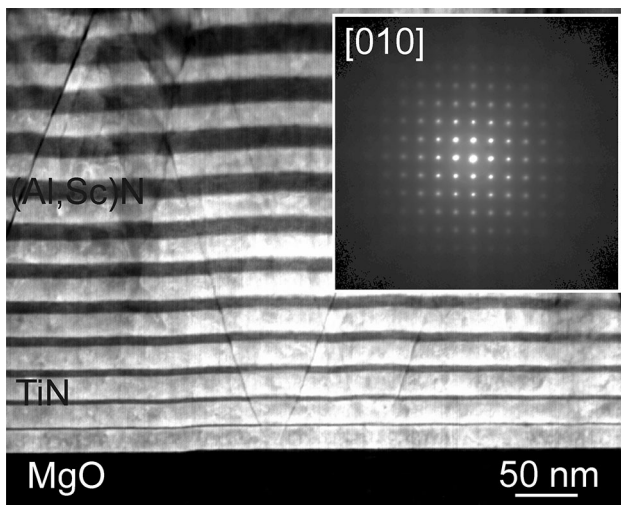


Figure 1 Low-magnification overview STEM micrograph with SAED of the TiN/(Al,Sc)N multilayer stack in the inset, confirming the epitaxial growth.

TEM sample preparation

A cross-sectional TEM lamella was prepared by focused ion beam (FIB) using a FEI Strata 400S system equipped with an OmniProbe 200 micromanipulator for in situ lift-out, where the lamella is transferred to copper TEM grids. The preparation was initially performed at 30 kV with an ion beam current of 21 nA. The lamella was thinned to about 100 nm thickness using ion beam currents from 0.44 nA down to 26 pA. The final thinning step was performed at 5 kV with 15 pA ion beam current. To improve the surface quality and to reduce the thickness further, the lamella was polished with a focused argon ion beam using a NanoMill system (Model 1040, Fischione Instruments). Ion energies from 900 eV down to 600 eV were used for 50 min in total to remove both the implanted Ga ions and the amorphous regions that formed during FIB preparation to prevent such effects influencing the EEL spectra [31].

Optical measurements

Dielectric permittivities of individual TiN (20 nm thickness) and $\text{Al}_{0.72}\text{Sc}_{0.28}\text{N}$ layers (thicknesses of 5 and 30 nm) were measured by spectroscopic ellipsometry (J. A. Woollam Co.). The ψ and δ plots were obtained for three different incidence angles, 30°, 50°, and 70°, respectively, in the spectral range of 320–2000 nm with an interval of 10 nm. The ellipsometry data were fitted with a Drude model for TiN and a Drude–Lorentz model for the (Al,Sc)N layers (see supplementary information Figure S2). No variation in permittivity was found between the 5 and 30 nm film thicknesses.

Results and discussion

Structurally, plasmonic metamaterials are characterized by a metal/dielectric interface with accompanying abrupt negative to positive transition of the real part of dielectric permittivity. Figure 2 shows the real and imaginary part of the dielectric permittivities of the TiN and $\text{Al}_{0.72}\text{Sc}_{0.28}\text{N}$ films, respectively, demonstrating that TiN becomes plasmonic with negative real permittivities (ϵ') above 500 nm spectral range. Due to its lower carrier concentration and mobilities with respect to the noble metals such as Au

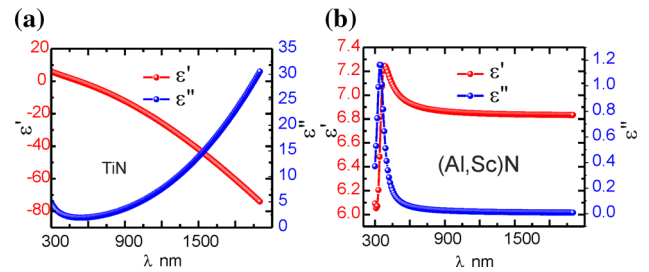


Figure 2 Real (ϵ') and imaginary (ϵ'') parts of the dielectric permittivity as a function of wavelength for the TiN (a) and (Al,Sc)N (b) films examined in this work as measured by variable angle spectroscopic ellipsometry. While ϵ' of TiN is negative above wavelengths of ~ 500 nm, ϵ' of (Al,Sc)N stays positive over the whole frequency range.

and Ag (the carrier concentration of sputter deposited TiN thin film is about $3.3 \times 10^{22} \text{ cm}^{-3}$, while traditional plasmonic materials like Au and Ag have carrier concentrations in the 5.9×10^{22} – $8 \times 10^{22} \text{ cm}^{-3}$ ranges), the ϵ' of TiN decreases rather slowly [29].

The imaginary part of the dielectric permittivity is dominated by interband transitions in the visible spectral range, while free electron Drude absorption dominates the ϵ'' at longer wavelengths. $\text{Al}_{0.72}\text{Sc}_{0.28}\text{N}$ thin films on the other hand show dielectric behavior in the visible to near IR spectral range and very low optical losses above 550 nm spectral ranges.

Figure 3a shows a high-angle annular dark-field (HAADF) STEM micrograph of the base part of the multilayer stack in cross-sectional view. The TiN layers appear bright with respect to the (Al,Sc)N due to the Z-contrast (contrast proportional to the atomic number of elements) produced with this technique. The layers appear mostly (but not perfectly) flat with sharp interfaces in the field of view, although further away from the substrate the structure can be seen to start becoming distorted (upper edge). The intended individual layer thicknesses were 20 nm for all TiN and 2 nm (increased in steps of 2 nm with each additional layer) for (Al,Sc)N. This is well reproduced for at least the first 10 periods of layer growth, which includes the entire region investigated by EELS.

A few defects can be found running diagonally from the substrate/film interface upward. The inset shows an atomically resolved STEM micrograph of a region across two interfaces marked by a rectangle, demonstrating the high quality of epitaxial growth for the second TiN/(Al,Sc)N interface, while further

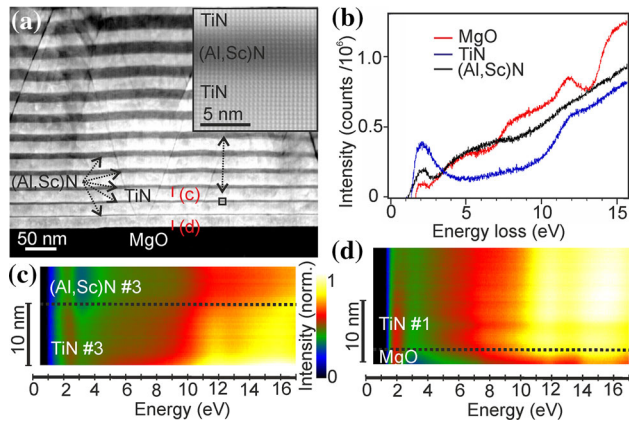


Figure 3 Overview STEM micrograph of the multilayer stack with constant TiN and systematically increasing $\text{Al}_{0.72}\text{Sc}_{0.28}\text{N}$ layer thicknesses. The inset shows the interface region marked by a rectangle at atomic resolution, demonstrating the high epitaxial growth quality (a). High-resolution EELS spectra from bulk regions of TiN, $\text{Al}_{0.72}\text{Sc}_{0.28}\text{N}$, and MgO are shown in (b). EELS line scans across the interfaces [marked by red lines in (a)] of TiN and (Al,Sc)N (c), and MgO and the first TiN layer (d) show the associated spectral changes in the low-loss regions after subtraction of the zero-loss peak (ZLP).

away from the substrate with increase in (Al,Sc)N thickness, more edge dislocations stemming from the slight lattice mismatch are to be found.

High-resolution low-loss EELS spectra have been taken in the bulk regions of individual TiN and (Al,Sc)N layers as well as in the substrate away from the interface for comparison (Fig. 3b). Care was taken that all EELS line scans were recorded far away from the diagonal defects, to rule out any effect that those might have on the plasmon resonances. Their potential influence will be investigated in a future study. A sharp edge associated with the TiN bulk plasmon energy can be seen in the spectral region between 2 and 3 eV. In order to map continuous changes in the plasmon resonance, spatially resolved EELS maps were recorded by scanning the beam across the interfaces of adjacent layers, and Fig. 3c, d shows such integrated scans taken along the red lines marked in (a). The scan in (c) extends from the central (bulk) region of the third TiN layer over the interface to the upper (Al,Sc)N layer. The plasmon resonance can be seen to become reduced from a bulk value of about ~ 2.5 eV toward the interface where the surface plasmon is located. Similarly, a slight change in plasmon energy is observed in the scan across the interface from the MgO substrate toward the first TiN layer (d).

High-resolution interface scans showing the plasmon resonances in the energy region corresponding to the spectral range of visible light (ca. 1.7–3.0 eV) are shown in Fig. 4.

The scan in Fig. 4a shows an increase in plasmon energy across the MgO/TiN interface in the direction

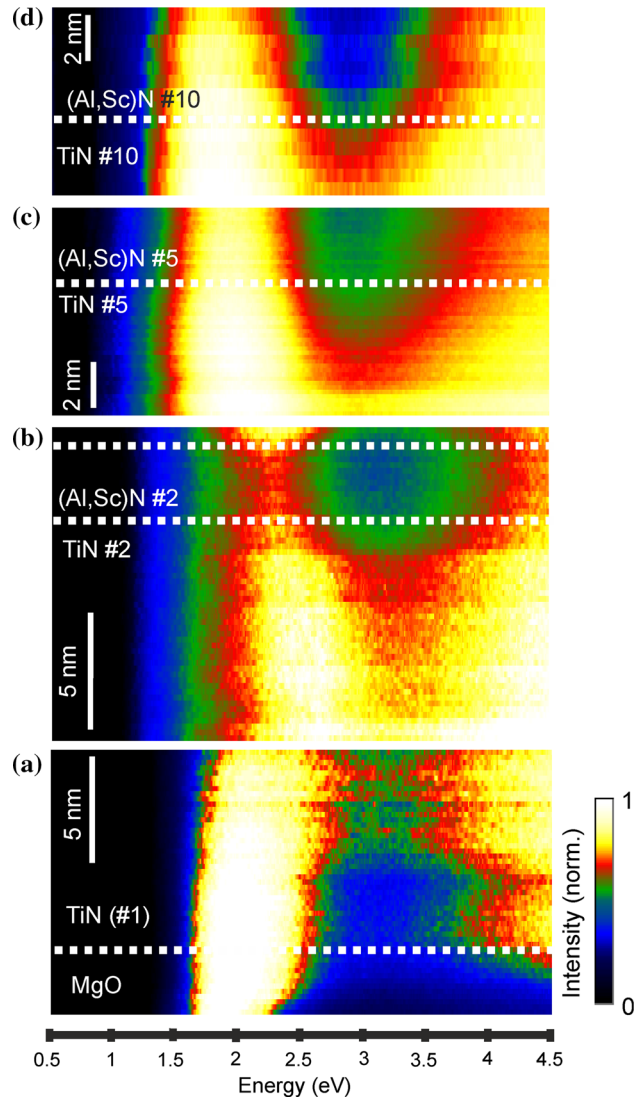


Figure 4 Integrated EELS scans across several multilayers interfaces show the changes from TiN bulk to surface plasmon resonance for different thicknesses of the (Al,Sc)N interlayer. Across the substrate/TiN layer interface, the plasmon resonance is observed to continuously shift to higher energy values toward the bulk (a). Similarly, the TiN surface plasmon energy is slightly lower at the TiN/(Al,Sc)N interface as compared to the TiN bulk resonance (b). With increasing (Al,Sc)N interlayer thickness (c, d), the differences between TiN bulk and surface plasmon resonances increase significantly. Layers are enumerated as grown from the substrate upward.

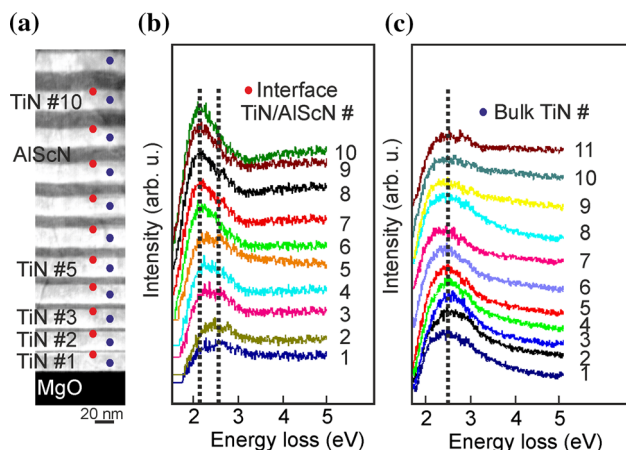


Figure 5 Waterfall plots of single EELS spectra taken from the region of interest shown in the STEM micrograph in (a): surface (b) and bulk (c) TiN inelastic scattering profiles after background subtraction showing a systematic reduction in surface plasmon resonance energy with increasing (Al,Sc)N interlayer thickness (b), while the TiN bulk plasmon resonances show no systematic changes (c).

away from the substrate. Directly at the interface, the intensity maximum can be found at about 2.2 eV, which corresponds well with other studies where a value of 2.15 eV has been reported for the MgO/TiN interface [17]. The interface scans across the second TiN/(Al,Sc)N (4 nm (Al,Sc)N) sequence (b) show a slight decrease in energy from the TiN bulk plasmon at ~ 2.5 eV toward the surface plasmon. Noticeably, the surface plasmon resonance is shifting gradually toward lower values for the fifth (c) and tenth (d) layer period of the stack. There, the (Al,Sc)N interlayer thicknesses are 10 nm (c) and 20 nm (d), the latter being equal to that of the TiN.

To verify the trend apparent in the line scans, ZLP subtracted single spectra that have been taken in the center of the TiN layers and close to the upper TiN/(Al,Sc)N interface are plotted in Fig. 5. The positions where the spectra have been taken are marked by dots in the overview HAADF-STEM micrograph (a).

From the interface spectra shown in the waterfall plot of Fig. 5b, the shift of TiN surface plasmon energy toward lower values with increasing (Al,Sc)N thicknesses becomes apparent (energy difference marked by two dotted lines), while the bulk plasmon

energies taken at the center of the TiN layers do not show systematic variation (c). For quantification, Gauss profiles were fit to each individual surface plasmon edge of Fig. 5b, and their maximum values (with a standard deviation of about 5 meV) are listed in Table 1. The supplementary information Figures S3 and S4 show the background subtraction from the raw data and the Gauss fitting on all interface spectra.

As can be seen, the TiN surface plasmon resonance decreases continuously with increasing interlayer thicknesses and converges at a value of 2.16 eV for interlayer thicknesses above 16 nm. One possibility for the bulk-like values of the surface plasmon for interlayer thicknesses in the range of a few nanometers is suggested in the literature [32]: Here, the authors describe the resonant coupling of surface and bulk plasmons that occurs at the interface of a metal and a dielectric, affecting the propagation of the surface plasmon polaritons. It is shown that a large part of the energy guided by the surface plasmon polaritons is transmitted through the resonance to the bulk plasmons, leading to a damping of the surface plasmon polaritons. How exactly the increase in (Al,Sc)N thickness weakens the coupling and strengthens the damping effect on the surface plasmon polaritons remains to be examined in another study, but we point out that similar damping on the surface plasmon polaritons at metal/dielectric interfaces has been demonstrated previously already [30]. Since the wavelength of light that is needed to excite plasmons in the energy range of 2.5–2.15 eV is between 500 and 575 nm, these resonances can be stimulated by light of the visible spectrum.

Similarly, the bulk plasmon edges were fit with Gaussians and found to have a mean average of 2.50 eV with a standard deviation of 0.05 eV. This value is independent of the (Al,Sc)N interlayer thickness. Others have recently reported the TiN bulk plasmon at an energy of 2.74 eV using STEM-EELS and an almost identical experimental setup and energy resolution as used in the present study [17]. Those values were, however, obtained from single TiN films with a thickness above 100 nm, while the TiN films in our study are only 20 nm thick. It can be

Table 1 TiN surface plasmon energy E_p as function of (Al,Sc)N interlayer thickness t

t (nm)	2	4	6	8	10	12	14	16	18	20
E_p (eV)	2.56	2.55	2.43	2.34	2.30	2.26	2.19	2.17	2.16	2.16

assumed, that at such thickness, the plasmon observed in the center of the film has not fully reached a bulk-like character, but still couples with the surface plasmons of lower energy. Another explanation for the small discrepancy could be slight differences in stoichiometry; however, as described in the “**Experimental**” section, we have determined the composition to be TiN_x with $x = 1$ (with an error of slightly below 2%) by EDS measurements.

Conclusions

The influence of semiconductor interlayer thicknesses on the bulk and surface plasmons of TiN in thin-film multilayers with systematically increasing (Al,Sc)N interlayer thicknesses has been investigated. While the TiN bulk plasmon keeps a constant value of about 2.50 eV, the surface resonance continuously decreases with increasing interlayer thickness until converging at about 2.16 eV once the interlayer reaches a thickness comparable to the one of TiN. This effect can be understood to be the result of resonant coupling between the TiN bulk and surface plasmons across the dielectric interlayers at very low (Al,Sc)N thicknesses. The detected plasmon resonance energies correspond to wavelengths between 500 and 575 nm, i.e., in the visible light range of the electromagnetic spectrum. Our results show that by carefully controlling the (Al,Sc)N interlayer thickness in the multilayer stack, TiN surface plasmon energies can be tailored, potentially enhancing the efficiency of solar energy-harvesting devices.

Supplementary information

A supplementary information file is provided online (see Electronic supplementary material) containing (1) raw data and details on the EDS mapping and analysis procedure, (2) ellipsometry raw data and fitting, and (3) EEL spectra background subtraction and Gauss fitting of all individual interface peaks to determine the position of E_p .

Acknowledgements

The Knut and Alice Wallenberg (KAW) Foundation is acknowledged for the Electron Microscope

Laboratory in Linköping. M.G. and L.H. acknowledge financial support from the Swedish Research Council [RÅC Frame Program (2011-6505), Project Grant 2013-4018, and Linnaeus Grant (LiLi-NFM)] as well as the Swedish Government Strategic Research Area in Materials Science on Functional Materials at Linköping University (Faculty Grant SFO-Mat-LiU 2009-00971). B.S. and T.D.S. acknowledge financial support from the National Science Foundation and U.S. Department of Energy (Award No. CBET-1048616). M.G. and B.S. acknowledge support from the Swedish Foundation for International Cooperation in Research and Higher Education (STINT). M.G. acknowledges support in specialized TEM sample preparation at the Karlsruhe Nano Micro Facility (Project ID 2015-015-010151) via V.S.K. Chakravadhanula.

Authors contribution

The manuscript was written through contributions of all authors. All authors have given approval to the final version of the manuscript. M.G. planned this study and carried out all TEM experiments, data analysis and plotting, and prepared all figures, and wrote the manuscript. L.H. and T.D.S. read and commented on the manuscript. M.H.F. prepared TEM samples and read and commented on the manuscript. B.S. conceptualized the research, performed sample growth, and read and commented on the manuscript.

Compliance with ethical standards

Conflict of interest The authors declare no competing financial interest.

Electronic supplementary material: The online version of this article (<https://doi.org/10.1007/s10853-017-1837-4>) contains supplementary material, which is available to authorized users.

Open Access This article is distributed under the terms of the Creative Commons Attribution 4.0 International License (<http://creativecommons.org/licenses/by/4.0/>), which permits unrestricted use, distribution, and reproduction in any medium, provided you give appropriate credit to the original author(s) and the source, provide a link to the

Creative Commons license, and indicate if changes were made.

References

- [1] Maier SA (2007) Plasmonics: fundamentals and applications. Springer, New York
- [2] Stockman MI (2011) Nanoplasmonics: past, present, and glimpse into future. *Opt Express* 19:22029–22106
- [3] Atwater HA (2007) The promise of plasmonics. *Sci Am* 296:56–62
- [4] Nie S, Emory SR (1997) Probing single molecules and single nanoparticles by surface-enhanced Raman scattering. *Science* 275:1102–1106
- [5] Zhang Y, Zhen YR, Neumann O, Day JK, Nordlander P, Halas NJ (2014) Coherent anti-stokes Raman scattering with single-molecule sensitivity using a plasmonic fano resonance. *Nat Commun* 5:4424
- [6] Morton J, Day E, Halas N, West J (2010) Nanoshells for photothermal cancer therapy. In: Grobmyer R, Moudgil BM (eds) *Cancer nanotechnology*, vol 624. Humana Press, New York, pp 101–117
- [7] Atwater HA, Polman A (2010) Plasmonics for improved photovoltaic devices. *Nat Mater* 9:205–213
- [8] Aydin K, Ferry VE, Briggs RM, Atwater HA (2011) Broadband polarization-independent resonant light absorption using ultrathin plasmonic super absorbers. *Nat Commun* 2:517
- [9] Tian Y, Tatsuma T (2004) Plasmon-induced photoelectrochemistry at metal nanoparticles supported on nanoporous TiO₂. *Chem Commun* 16:1810–1811
- [10] Boltasseva A, Atwater HA (2011) Low-loss plasmonic metamaterials. *Science* 331:290–291
- [11] Guoliang L, Cherqui C, Bigelow NW, Duscher G, Straney PJ, Millstone JE, Masiello DJ, Camden JP (2015) Spatially mapping energy transfer from single plasmonic particles to semiconductor substrates via STEM/EELS. *Nano Lett* 15:3465–3471
- [12] Hylton NP, Li XF, Giannini V, Lee K-H, Ekins-Daukes NJ, Loo J, Vercautysse D, Van Dorpe P, Sodabanlu H, Sugiyama M, Maier SA (2017) Loss mitigation in plasmonic solar cells: aluminium nanoparticles for broadband photocurrent enhancements in GaAs photodiodes. *Sci Rep* 3:2874
- [13] Gong C, Leite MS (2016) Noble metal alloys for plasmonics. *ACS Photonics* 3(4):507–513
- [14] West PR, Ishii S, Naik GV, Emani K, Shalaev VM, Boltasseva A (2010) Searching for better plasmonic materials. *Laser Photonics Rev* 4:795–808
- [15] Guler U, Naik GV, Boltasseva A, Shalaev VM, Kildishev AV (2012) Performance analysis of nitride alternative plasmonic materials for localized surface plasmon applications. *Appl Phys B Lasers Opt* 107:285–291
- [16] Naik GV, Schroeder JL, Ni X, Kildishev AV, Sands TD, Boltasseva A (2012) Titanium nitride as a plasmonic material for visible and near-infrared wavelengths. *Opt Mater Express* 2:478–489
- [17] Herzing AA, Guler U, Zhou X, Boltasseva A, Shalaev V, Norris TB (2016) Electron energy loss spectroscopy of plasmon resonances in titanium nitride thin films. *Appl Phys Lett* 108:171107
- [18] Brongersma ML, Halas NJ, Nordlander P (2015) Plasmon-induced hot carrier science and technology. *Nat Nanotechnol* 10:25–34
- [19] Clavero C (2014) Plasmon-induced hot-electron generation at nanoparticle/metal-oxide interfaces for photovoltaic and photocatalytic devices. *Nat Photonics* 8:95–103
- [20] Ishii S, Laxman Shinde S, Jevasuwan W, Fukata N, Nagao T (2016) Hot electron excitation from titanium nitride using visible light. *ACS Photonics* 3(9):1552–1557
- [21] Sakhdari M, Hajizadegan M, Farhat M, Chen PY (2016) Efficient broadband and wide-angle hot-electron transduction using metal-semiconductor hyperbolic metamaterials. *Nano Energy* 26:371–381
- [22] Saha B, Lawrence SK, Schroeder JL, Birch J, Bahr DF, Sands TD (2014) Enhanced hardness in epitaxial TiAlScN alloy thin films and rocksalt TiN/(Al, Sc)N superlattices. *Appl Phys Lett* 105:151904
- [23] Saha B, Saber S, Naik GV, Boltasseva A, Stach EA, Kvam EP, Sands TD (2015) Development of epitaxial Al_xSc_{1-x}N for artificially structured metal/semiconductor superlattice metamaterials. *Phys Status Solidi B* 252(2):251–259
- [24] Schroeder JL, Saha B, Garbrecht M, Schell N, Sands TD, Birch J (2015) Thermal stability of epitaxial cubic-TiN/(Al,Sc)N metal/semiconductor superlattices. *J Mater Sci* 50:3200–3206. <https://doi.org/10.1007/s10853-015-8884-5>
- [25] Saha B, Koh YR, Comparan J, Sadasivam S, Schroeder JL, Garbrecht M, Mohammed A, Birch J, Fisher T, Shakouri A, Sands TD (2016) Cross-plane thermal transport in (Ti,W)N/(Al,Sc)N metal/semiconductor superlattices. *Phys Rev B*. 93:045311
- [26] Garbrecht M, Schroeder JL, Hultman L, Birch J, Saha B, Sands TD (2016) Microstructural evolution and thermal stability of HfN/ScN, ZrN/ScN, and Hf_{0.5}Zr_{0.5}N/ScN metal/semiconductor superlattices. *J Mater Sci* 51(17):8250–8258. <https://doi.org/10.1007/s10853-016-0102-6>
- [27] Garbrecht M, Saha B, Schroeder JL, Hultman L, Sands TD (2017) Dislocation-pipe diffusion in nitride superlattices observed in direct atomic resolution. *Sci Rep* 7:46092

- [28] Garbrecht M, Hultman L, Farwey MH, Sands TD, Saha B (2017) Void-mediated coherence-strain relaxation and impediment of cubic-to-hexagonal transformation in epitaxial metastable metal/semiconductor $\text{TiN}/\text{A}_{0.72}\text{Sc}_{0.28}\text{N}$ multilayers. *Phys Rev Mater* 01:033402
- [29] Saha B, Naik GV, Saber S, Stach E, Shalaev VM, Boltasseva A, Sands TD (2014) $\text{TiN}/(\text{Al},\text{Sc})\text{N}$ metal/dielectric superlattices and multilayers as hyperbolic metamaterial in the visible spectral range. *Phys Rev B* 90:125420
- [30] Naik GV, Saha B, Liu J, Saber SM, Stach EA, Irudayaraj JMK, Sands TD, Shalaev V, Boltasseva A (2014) Epitaxial superlattices with titanium nitride as a plasmonic component for optical hyperbolic metamaterials. *Proc Natl Acad Sci USA* 111:7546–7551
- [31] Mitome M (2013) Ultrathin specimen preparation by a low-energy Ar-ion milling method. *J Electron Microsc* 62(2):321–326
- [32] Akimov YA, Chu HS (2011) Plasmon coupling effect on propagation of surface plasmon polaritons at a continuous metal/dielectric interface. *Phys Rev B* 83:165412